J Mater Sci (2011) 46:4994–5001
DOI 10.1007/s10853-011-5418-7

Hot deformation of ultrafine-grained Al6063/Al_2O_3 nanocomposites

H. Asgharzadeh · A. Simchi · H. S. Kim

Received: 24 October 2010 / Accepted: 25 February 2011 / Published online: 8 March 2011

Abstract Ultrafine-grained (UFG) Al6063 alloy reinforced with 0.8 vol% nanometric alumina particles (25 nm) was prepared by reactive mechanical alloying and direct powder extrusion. Transmission electron microscopy and electron backscatter diffraction analysis showed that the grain structure of the nanocomposite composed of nanosize grains (<0.1 μm), ultrafine grains (0.1–1 μm) and micron-size grains (>1 μm) with random orientations. Mechanical properties of the material were examined at room and high temperatures by compression test. It was found that the yield strength of the UFG composite material is mainly controlled by the Orowan mechanism rather than the grain boundaries. The deformation activation energy at temperature ranges of $T < 300$ °C and 300 °C $\leq T < 450$ °C was determined to be 74 and 264 kJ mol^{-1}, respectively. This observation indicated a change in the deformation mechanism at around 300 °C. At the higher temperatures, significant deformation softening was observed due to dynamic recrystallization of non-equilibrium grain boundaries. The reinforcement nanoparticles, however, renders the high strength of the material at the elevated temperatures mainly by dislocation pinning.

H. Asgharzadeh · A. Simchi
Department of Materials Science and Engineering, Sharif University of Technology, Azadi Avenue, P.O. Box 11365-9466, Tehran, Iran

A. Simchi (✉)
Institute for Nanoscience and Nanotechnology, Sharif University of Technology, Azadi Avenue, P.O. Box 11365-9466, Tehran, Iran
e-mail: simchi@sharif.edu

H. S. Kim
Department of Materials Science and Engineering, Pohang University of Science and Technology, Pohang 790-784, South Korea

Introduction

Particle-reinforced aluminum matrix composites (AMCs) are used for numerous applications in automotive, aerospace, and defense industries as well as electronic packaging and sporting goods [1]. The wide applications of AMCs are due to the combination of suitable properties including low weight, high electrical and thermal conductivity, low thermal expansion, high specific strength and stiffness, good wear resistance, and environmental corrosion resistance [2]. Further improvement in the mechanical properties may be achieved by decreasing the grain size of the aluminum matrix as well as the size of reinforcement particles. Qian et al. [3] showed that yield strength of coarse-grained Al6063 can be increased ~150% through grain refinement to ultrafine range via employing severe plastic deformation. Kang and Chan [4] reported that the tensile properties of Al–1 vol% Al_2O_3 (25 nm) was comparable to that of Al–10 vol% SiC (10 μm).

Another advantage of reinforcing aluminum alloys with ceramic nanoparticles is related to rendering high-temperature strength. It is well known that grain coarsening and dissolution of fine precipitates at higher temperatures degrade the strength of aluminum alloys and thus limit their application [5, 6]. The presence of thermally stable nanoparticles in the matrix improves the strength and microstructural stability of aluminum alloys. Zhang et al. [7] showed that hot compressive strength of Al2024–20 vol% SiC is improved by replacing 3 vol% micronsize SiC whiskers with nanosize SiC particles. Superior compressive yield

strength of Al–5 vol% Al_2O_3 at elevated temperatures compared to monolithic Al has also been reported by Razavi Hessabi et al. [5]. Meanwhile, particular attention should be paid to agglomeration and non-uniform dispersion of the reinforcement particles through the matrix, particularly when a high volume fraction of the ceramic particles are utilized. Many researchers [8–14] have utilized mechanical alloying (MA) process to fabricate nanostructured aluminum matrix nanocomposites. Both ex situ synthesis (blending nanometric-size reinforcement particles with aluminum powder) and in situ synthesis (using chemical reactions to form the reinforcement particles) have been examined. Besides uniform distribution of the reinforcement particles throughout the aluminum matrix, severe plastic deformation during mechanical alloying results in a significant grain refinement and ultimately the formation of nanostructured material. Nevertheless, the subsequent consolidation step by means of various thermomechanical processes [15] alters the microstructural features of the nanocomposite material and affects its mechanical properties and performance. We have recently shown that mechanical alloying of Al6063 alloy in an oxygen-rich atmosphere followed by hot extrusion yields ultrafine-grained nanocomposite with bimodal grain structure, possessing interesting properties [16]. In this study, the hot deformation behavior of the nanocomposite is presented and compared with coarse-grained Al6063 alloy. Results of available reports [5, 7, 17] on the hot deformation aluminum matrix nanocomposites have revealed interesting features of the hot deformation behavior of these materials with regard to dynamic recovery and recrystallization that need to be explored in details.

Experimental procedure

Gas-atomized Al6063 powder (Al–0.64 Mg–0.67Si–0.32Fe–0.2Cu; in wt%) was used as starting material. The average size of Al6063 particles was about 71 μm. A mixture of Al6063 and 1.5 wt% stearic acid (Merck, Germany) powders was prepared by 20 min blending in a Turbula shaker/mixer (Willy A. Bachofen, Basel, Switzerland) and mechanically milled in a high-energy attrition ball mill (Union Process, Inc., USA). For accomplishment of in situ reaction, mechanical milling was performed under a Ar–5 vol% O_2 atmosphere. Blowing of the gas into the vial was exactly controlled by mass flow controllers (Brookes Instrument, USA). The milling process was continued up to 20 h. Rotational speed of 400 rpm was used. The ball-to-powder charge ratio of 10:1 was utilized. The milled powder was degassed in a vacuum furnace at 400 °C for 1 h and then pre-compacted in an aluminum container at pressure of 200 MPa. After sealing, the aluminum container was pre-heated at 450 °C under an argon atmosphere and finally extruded at the ratio of 14:1 and speed of 1 mm s^{-1}. To fabricate coarse-grained Al6063 specimens, the gas-atomized powder was degassed and consolidated according to the same procedure without performing the mechanical milling stage.

The microstructure of the prepared billets was studied by electron backscatter diffraction (EBSD) and transmission electron microscopy (TEM) parallel to the extrusion direction. For EBSD observations, after mechanical grinding and pre-polishing of the specimens, the films were ion-milled in a PIPS (Model 691, Gatan, Inc., USA) just before EBSD analysis. Acquisition of EBSD data was performed using a 3D total analysis (Helios NanoLab DualBeam, FEI, USA) equipped with a high-resolution EBSD detector (Hikari, EDAX, USA). Orientation mapping was made on a rectangular grid with a step size of 20 nm. The corresponding data processing was then carried out using OIM analysis software (version 5.2, EDAX, USA). Thin TEM foils were prepared by grinding and polishing methods. After punching to 3 mm diameter disks, dimple grinding (Model 656, Gatan, Inc., USA) was performed. Final thinning was carried out by ion-milling using PIPS instrument until perforation. TEM observations were done by JEM-2100F STEM (JEOL, Japan) operated at 200 kV. The volume fraction of the particles was measured by linear intercept method from TEM images. The size of particles was determined from the TEM images by measurement of the size of more than 20 particles. The dislocation density was estimated by the line intercept method by considering the foil thickness of 100 nm.

To examine the mechanical strength, compression test was performed. Cylindrical specimens with diameter of 4 mm and height of 5 mm were machined from the extruded billet along the extrusion direction by electro-discharge machining method. The surfaces of the specimens were finely polished by diamond pastes. Compression test was performed in a Caster and Thermomechanical Simulator (Fuji Electronic Industrial Co., Ltd., Japan) machine. The compression tests were carried out at temperatures ranging from 25 to 450 °C. Strain rates of 0.01–1 s^{-1} were applied. Quartz plates were used for lubricating the anvils. The specimens were quenched immediately after finishing test to preserve the microstructure. The microstructure of the deformed samples was examined by EBSD and TEM.

Results

Figure 1a shows the EBSD inverse pole figure (IPF) map of Al6063/Al_2O_3 nanocomposite. The microstructure

consists of a mixture of nanosize grains (<0.1 μm), ultrafine grains (0.1–1 μm), and micronsize grains (>1 μm) with random orientations. Grain size distribution obtained from EBSD analysis (Fig. 1c) shows that most of the grains are in the submicron (ultrafine) range and only low fraction of nanosize and micronsize grains exist in the microstructure (Fig. 1b). The grain structure is similar to 6XXX aluminum alloys and their composites processed via severe plastic deformation techniques [18–21]. While larger grains (approx. >0.5 μm) are relatively elongated in the extrusion direction, smaller grains (approx. <0.5 μm) are almost equiaxed (Fig. 1a). The average aspect ratio is about 1.7. Figure 1d illustrates the frequency distribution of misorientation angles for Al6063/Al_2O_3 nanocomposite. The misorientation (θ) distribution shows the presence of low-angle grain boundaries ($2° < \theta < 15°$) as well as high-angle grain boundaries ($\theta > 15°$). The low- and high-angle grain boundaries are detectable in Fig. 1a through white and black lines, respectively. As seen, the majority of grain boundaries are high-angle type; their fraction is about 64% with an average misorientation angle of 27°. More details of the microstructural features are revealed in the STEM image shown in Fig. 2. The microstructure consists of relatively equiaxed grains/subgrains with ultrafine size in agreement with the EBSD results (Fig. 1). While high density of dislocations can be seen in relatively large grains, smaller grains are characterized by low density of dislocations. It is pertinent to point out that nanostructured grains are relatively dislocation free. It is known that when the grain size is smaller than a critical value, the mean free path of dislocations is limited only by its grain boundaries [22]. Therefore, the nanostructured grains are likely out of dislocation forest and tangling. From Fig. 2, one can also notice a relatively uniform distribution of precipitates and reinforcement particles in the Al6063 matrix. The precipitate particles have irregular shape with an average size of ~80 nm. As shown elsewhere [23, 24], these particles have the composition of Al_5FeSi, Al_8Fe_2Si, and $Al_8Mg_3FeSi_2$.

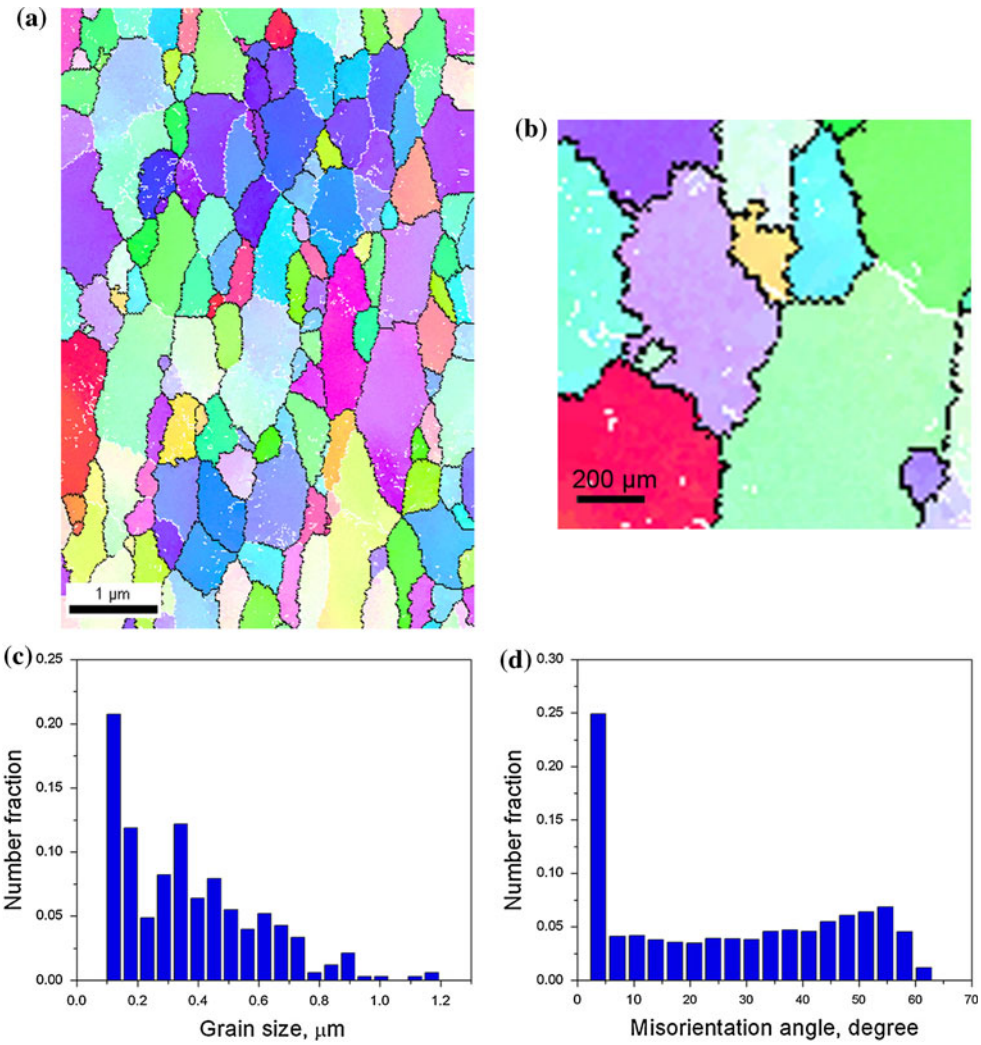

Fig. 1 **a** EBSD inverse pole figure map, **b** EBSD map from a small region at higher magnification, **c** grain size distribution, and **d** misorientation angle distribution for Al6063/Al_2O_3 nanocomposite

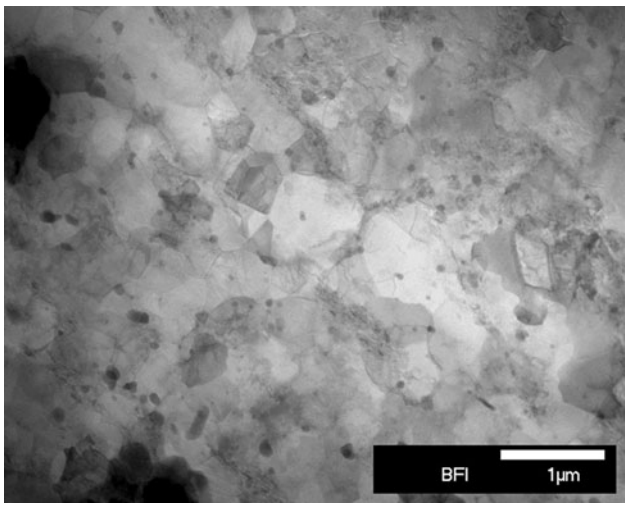

Fig. 2 STEM image showing the microstructure of Al6063/Al_2O_3 nanocomposite

The reinforcement particles are amorphous alumina with an average size of ~25 nm. The volume fraction of the reinforcement is ~0.8%.

The compressive true stress–strain curves of Al6063 alloy and the nanocomposite at 25 and 450 °C are shown in Fig. 3. The superior mechanical strength of the nanocomposite compared to that of Al6063 alloy at room temperature is a result of nanometric reinforcement particles and the ultrafine grain structure. It is noteworthy that the obtained mechanical properties are superior to those reported for ultrafine-grained Al6063 alloy [3] and Al6061Al–10 vol% Al_2O_3 composite [21] processed by severe plastic deformation as well. The flow stress of the both materials exhibit a significant decrease at the high temperature compared to the room temperature deformation. The values of the peak flow stress at different testing temperatures are shown in Fig. 3b. A limited initial strain hardening region followed by a slight decrease in the flow stress, i.e., strain softening, is also visible in Fig. 3a. To investigate the restoration mechanism involved in the hot deformation process, EBSD and TEM studies were performed. Figure 4a shows EBSD-IPF map for the nanocomposite after deformation at 300 °C with a strain rate of 1 s^{-1}. One can notice that the elongated large grains in the as-extruded specimen (Fig. 1a) were replaced by equiaxed grains, revealing a significant grain size refinement during hot deformation (see Fig. 4b). On the other hand, Fig. 4c determines that highly misoriented boundaries with an average misorientation angle of 31° were formed. The fraction of high-angle boundaries also increased to 75%. Figure 5 shows that small and equiaxed grains with relatively low density of dislocations were also formed. All these evidences support the occurrence of dynamic recrystallization during hot deformation. It was worthy to

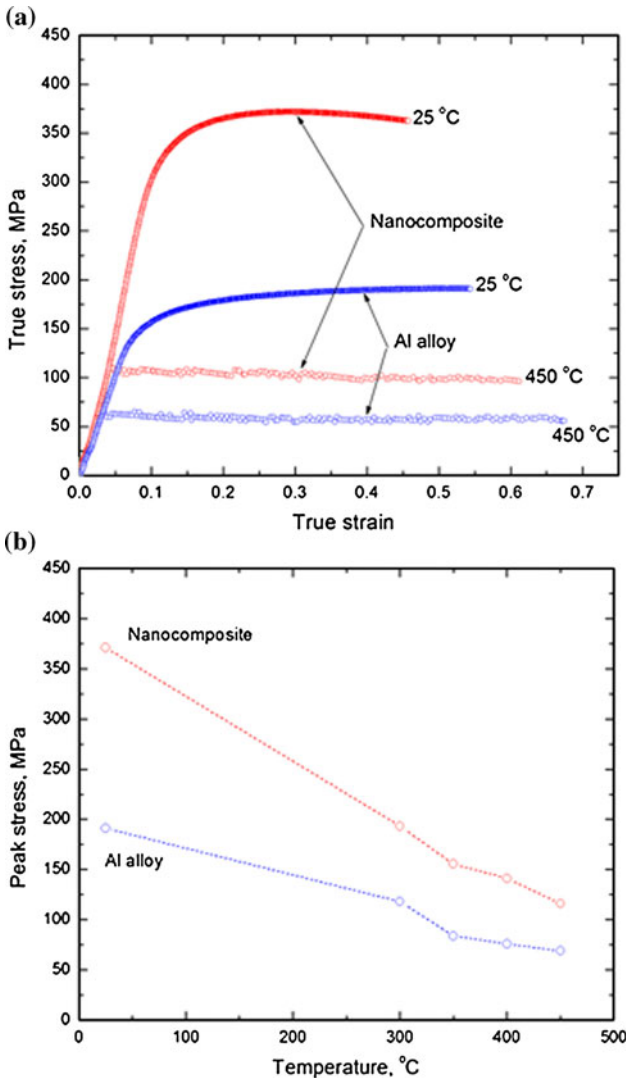

Fig. 3 **a** True stress–strain curve and **b** flow stress of Al6063 alloy and Al6063/Al_2O_3 nanocomposite depending on the deformation temperature. The strain rate is 1 s^{-1}

mention that no remarkable difference in the fraction and distribution of the second phases could be observed.

Discussion

A significant increase in the compressive yield stress and ultimate strength of coarse-grained Al6063 alloy was obtained by employing the reactive mechanical alloying process followed by hot extrusion. This is attributed to the coupled effects of (a) grain refinement, (b) the presence of alumina nanoparticles and their effect on load bearing and dislocations glide, (c) thermal mismatch dislocations, and (d) geometrically necessary dislocations. The coupled effects can be theoretically described by an unified model [25, 26] or the summation of the separate effects. For the

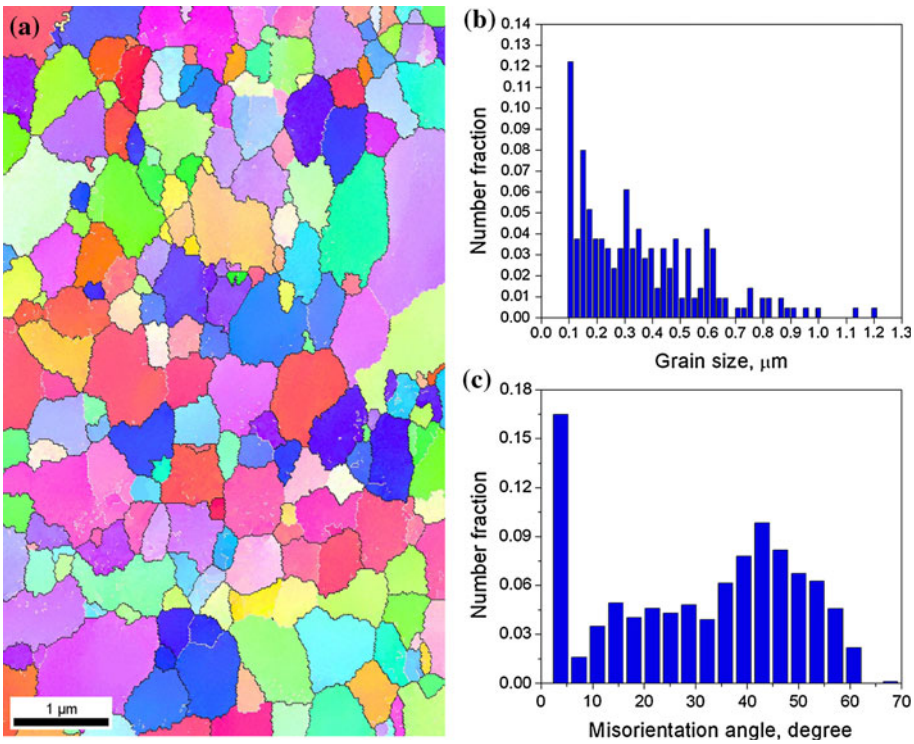

Fig. 4 **a** EBSD-IPF map, **b** grain size distribution, and **c** misorientation angle distribution of Al6063/Al_2O_3 nanocomposite after compression at temperature of 450 °C and strain rate of 1 s^{-1}

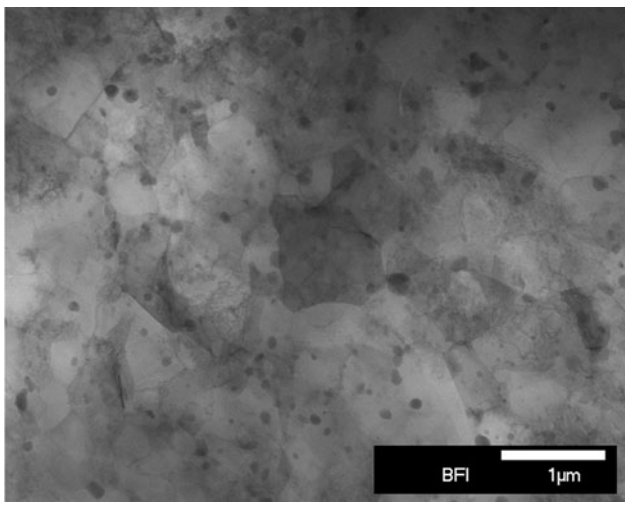

Fig. 5 STEM image showing the microstructure of hot-deformed Al6063/Al_2O_3 nanocomposite at 300 °C with a strain rate of 1 s^{-1}

latter approach, a general equation for prediction of yield stress is [27]:

$$\sigma = \sigma_{ss} + \left(\sigma_{gs}^m + \sigma_{dis}^m + \sigma_{disper}^m\right)^{1/m}, \quad (1)$$

where σ_{ss} is solid solution strengthening, σ_{gs} grain size strengthening, σ_{dis} dislocation strengthening, σ_{disper} dispersion strengthening, and m a constant that can vary between 1 (linear superposition) and 2 (Pythagorean superposition). By assuming that most of the solute atoms were depleted from the matrix into the precipitates and considering the Hall-Petch equation [28, 29], Taylor relationship [30], and Orowan mechanism [31] as strengthening mechanisms, it can be written as:

$$\sigma_{ss} = \sigma_0 \quad (2)$$

$$\sigma_{gs} = k/\sqrt{D} \quad (3)$$

$$\sigma_{dis} = \alpha G b \sqrt{\rho} \quad (4)$$

$$\sigma_{disper} = \frac{0.4GbM}{\pi\sqrt{1-\nu}} \frac{\ln\left(\sqrt{\frac{2}{3}}\frac{d}{b}\right)}{\left(\sqrt{\frac{2}{3}}\frac{d}{b}\right)\left(\sqrt{\frac{\pi}{4f}-1}\right)}. \quad (5)$$

The parameters used in these equations are defined in Table 1. The results presented in Table 2 indicate that:

- The yield strength of the nanocomposite can be predicated by linear superposition ($m = 1$) of different strengthening mechanisms
- The Orowan mechanism plays a significant role on the strengthening of the nanocomposite. This implies that the reinforcement nanoparticles could effectively pin the dislocations
- High fraction of grain boundaries has remarkably contributed to the strengthening by limiting the mean free path of dislocations.

As similar to pure materials and metal alloys, the strength of the ultrafine-grained Al6063–Al_2O_3 nanocomposite decreased with increasing the deformation temperature. This observation indicates that thermally activated

Table 1 Definition and values of the parameters used in Eqs. 2–5

Parameters	Definition	Value
σ_0	Lattice friction stress	50 MPa[a]
k	Locking parameter	70 MPa$\sqrt{\mu m}$[a]
D	Matrix grain size	480 nm
α	Constant	0.3[a]
G	Shear modulus	25.8 GPa[a]
b	Burgers vector	0.286 nm[a]
ρ	Dislocation density	1.5×10^{14} m^{-2}
M	Taylor factor	3.06[a]
v	Poisson's ratio	0.33[a]
d	Diameter of dispersoids	Reinforcement: 25 nm precipitate: 80 nm
f	Volume fraction of dispersoids	Reinforcement: 0.008 precipitate: 0.036

[a] Extracted from references [32, 33]

Table 2 Calculation of the different sources of strengthening mechanism for Al6063–0.8 vol% Al_2O_3 nanocomposite according to Eq. 1

Strengthening mechanism	Strength induced by (MPa)
Friction stress (σ_0)	50
Grain refinement (σ_{gs})	101
Dislocations (σ_{dis})	27
Precipitates (σ_{pt})	79
Reinforcement nanoparticles (σ_r)	63
Predicated yield strength for $m = 1$	320
Predicated yield strength for $m = 2$	195
Yield strength (experimental)	320

mechanisms were involved at the elevated temperatures. The relationship between the maximum flow stress (σ_p), temperature (T), and strain rate ($\dot{\varepsilon}$) during hot deformation is commonly expressed by [34]:

$$\dot{\varepsilon} = A\sigma_p^n \exp\left(-\frac{Q}{RT}\right), \quad (6)$$

where Q is the apparent activation energy for deformation, R the gas constant (8.314 kJ mol^{-1}), and A and n are material parameters. Figure 6a shows the flow stress as a function of strain rate in log-scale. The slope of the lines gives $n = 0.04$. The value of the apparent activation energy for the hot deformation can also be calculated by [34]:

$$Q = nRS, \quad (7)$$

where S is determined from σ–$1/T$ graph (see Fig. 6b). The change in the slope of the lines with increasing the temperature implies that two different deformation mechanisms are operative. The apparent activation energy was

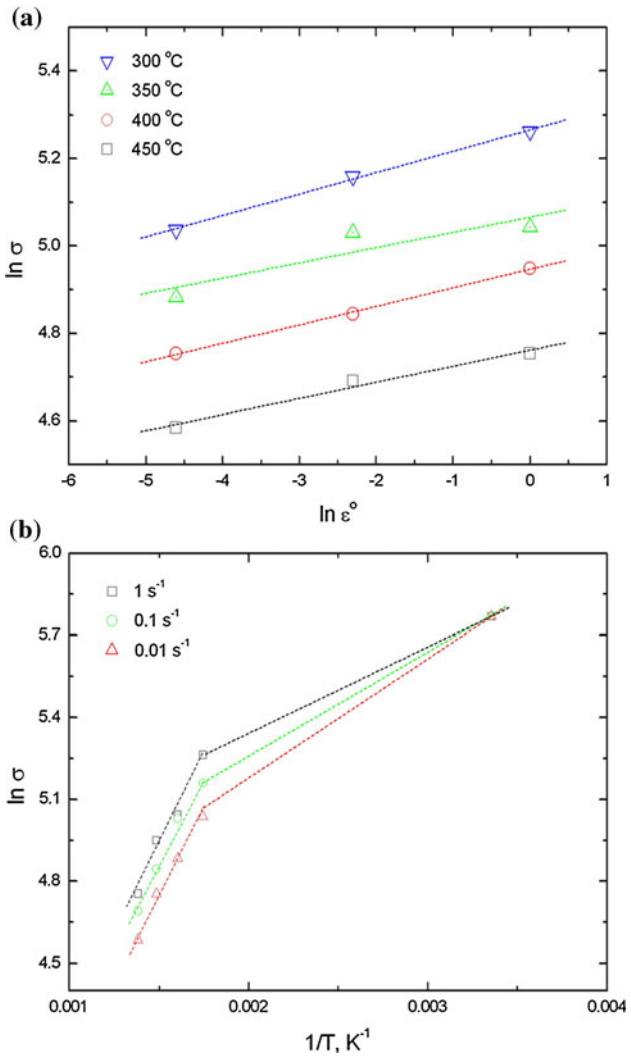

Fig. 6 Variation of the flow stress versus **a** strain rate and **b** temperature for Al6063–Al_2O_3 nanocomposite

found to be 78 kJ mol^{-1} at $T < 300$ °C and 264 kJ mol^{-1} at $T \geq 300$ °C. Increasing of the apparent activation energy by increasing the deformation temperature has also been observed for Al6061 alloy and Al6061–10 vol% Al_2O_3 composite [35, 36]. The value of activation energy at $T < 300$ °C is close to the grain boundary self-diffusion of Al (84 kJ mol^{-1} [37]) while the activation energy in the range of 200–260 kJ mol^{-1} [35–42] could imply the occurrence of dynamic recrystallization as evidenced by microstructural studies (Figs. 4, 5). In spite of dynamic restoration, the nanocomposite exhibited a remarkable strength at high temperatures (Fig. 3). This can be attributed to the dislocation pinning effect of the nanoparticles as shown in Fig. 7. The thermally stable reinforcement particles also hinder the grain growth of the aluminum matrix at elevated temperature to some extent as reported previously [5].

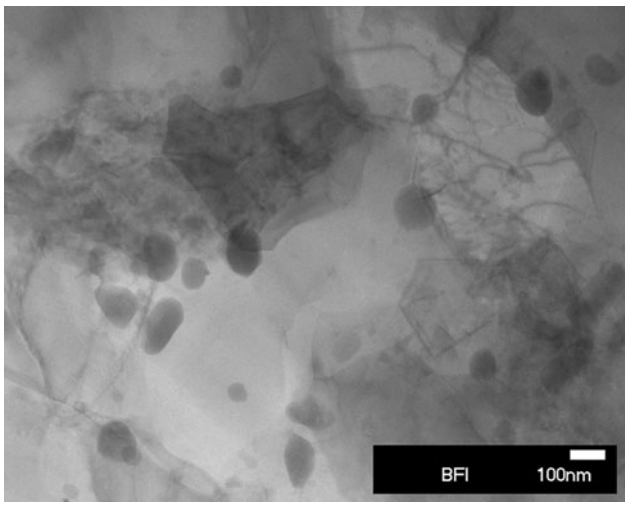

Fig. 7 STEM image showing the interaction of dislocations with the dispersoids in hot-deformed Al6063/Al_2O_3 nanocomposite at 300 °C with a strain rate of 1 s^{-1}

Conclusions

Ultrafine-grained Al6063/Al_2O_3 nanocomposite was produced by a combination of reactive mechanical milling and hot powder extrusion. The deformation behavior of the nanocomposite was studied at ambient and elevated temperatures. The findings can be summarized as follows:

- A duplex-grain structure consisting of nanoscale grains and ultrafine grains was formed after hot consolidation of the nanostructured aluminum alloy powder
- It was shown that Al_2O_3 particles with an average diameter of 25 nm were "in situ" formed during reactive mechanical milling
- The presence of large amount of high-angle grain boundaries (64%) in the microstructure was noticed. It was shown that the strength of the prepared Al6063/Al_2O_3 nanocomposite is significantly influenced by the nanosized alumina particles and the ultrafined grain structure
- Deformation at $T < 300$ °C is supported by dislocations cross slip with an activation energy of 78 kJ mol^{-1} which is close to that of the grain boundary self diffusion of aluminum. At $T \geq 300$ °C, the activation energy of deformation was determined to be 264 kJ mol^{-1}
- Dynamic recrystallization during hot deformation at the elevated temperatures was observed, which resulted in flow softening.

Acknowledgements HSK acknowledges the support by a grant from the Fundamental R&D Program for Core Technology of Materials funded by the Ministry of Knowledge Economy, Korea.

References

1. Smagorinski ME, Tsantrizos PG, Grenier S, Cavasin A, Brzezinski T, Kim G (1998) Mater Sci Eng A 244:86
2. Prabhu B, Suryanarayana C, An L, Vaidyanathan R (2006) Mater Sci Eng A 425:192
3. Qian T, Marx M, Schuler K, Hockauf M, Vehoff H (2010) Acta Mater 58:2112
4. Kang YC, Chan SL (2004) Mater Chem Phys 85:438
5. Razavi Hesabi Z, Sanjari M, Simchi A, Seyed Reihani SM, Simancik F (2009) J Nanosci Nanotechnol 9:1
6. Witkin D, Han BQ, Lavernia EJ (2005) J Mater Eng Perform 14:519
7. Zhang XN, Geng L, Xu B (2007) Mater Chem Phys 101:242
8. Wu JM (2000) J Alloy Compd 299:9
9. Wu JM (2001) Mater Lett 48:324
10. Kleiner S, Bertocco F, Khalid FA, Beffort O (2005) Mater Chem Phys 89:362
11. Moon KI, Lee KS (1998) J Alloy Compd 264:258
12. Moon KI, Lee KS (1998) J Alloy Compd 279:201
13. Cintas J, Cuevas FG, Montes JM, Herrera EJ (2005) Scr Mater 53:1165
14. Saji S, Yasuda H, Yamane T (1994) Mater Sci Eng A 179–180:676
15. Viswanathan V, Laha T, Balani K, Agarwal A, Seal S (2006) Mater Sci Eng R 54:121
16. Asgharzadeh H, Simchi A, Kim HS (2011) Metall Mater Trans A 42:816
17. Zhang Z, Han BQ, Zhou Y, Lavernia EJ (2008) Mater Sci Eng A 493:221
18. Ferrasse S, Segal VM, Hartwig KT, Goforth RE (1997) J Mater Res 12:1253
19. Horita Z, Fujinami T, Nemoto M, Langdon TG (2000) Metall Mater Trans 31A:691
20. Kim JK, Jeong HG, Hong SI, Kim YS, Kim WJ (2001) Scr Mater 45:901
21. Han BQ, Langdon TG (2005) Mater Sci Eng A 410–411:430
22. Li Y, Zhao YH, Ortalan V, Liu W, Zhang ZH, Vogt RG, Browning ND, Lavernia EJ, Schoenung JM (2009) Mater Sci Eng A 527:305
23. Asgharzadeh H, Simchi A, Kim HS (2011) Mater Sci Eng A. doi: 10.1016/j.msea.2011.01.082
24. Asgharzadeh H, Simchi A, Kim HS (2010) Mater Sci Eng A 527:4897
25. Estrin Y (1996) In: Krausz AS, Krausz K (eds) Unified constitutive laws of plastic deformation. Academic Press, New York, p 69
26. Kim HS, Bush MB, Estrin Y (2000) Mater Sci Eng A 276:175
27. Shanmugasundaram T, Heilmaier M, Murty BS, Subramanya Sarma V (2009) Metall Mater Trans A 40:2798
28. Hall EO (1951) Proc Phys Soc 643:747
29. Petch NJ (1953) J Iron Steel Inst 174:25
30. Dieter GE (1988) Mechanical metallurgy, SI metric edition. McGraw-Hill, London
31. Ye J, Han BQ, Lee Z, Ahn B, Nutt SR, Schoenung JM (2005) Scr Mater 53:481
32. Hardbound ACR (ed) (2001) Properties and selection: nonferrous alloys and special purpose materials, vol 2. ASM, Materials Park
33. Gutierrez-Urrutia I, Muñoz-Morris MA, Morris DG (2006) J Mater Res 21:329
34. Humphreys FJ, Haterly M (2004) Recrystallization and related annealing phenomena, 2nd edn. Elsevier, Oxford
35. Xia X, McQueen HJ, Sakaris P (1995) Scr Metall Mater 32:1185
36. Asgharzadeh H, Simchi A (2008) Powder Metall 51:354

37. Frost HJ, Ashby MF (1982) Deformation-mechanism maps. Pergamon Press, Oxford
38. Porter DA, Easterling KE (1992) Phase transformations in metals and alloys, 2nd edn. CRC Press, New York
39. Zhang H, Li L, Yuan D, Peng D (2007) Mater Charact 58:168
40. Ganesan G, Raghukandan K, Karthikeyan R, Pai BC (2004) Mater Sci Eng A 369:230
41. Xia X, Sakaris P, McQueen HJ (1994) Mater Sci Technol 16:487
42. Asgharzadeh H, Simchi A (2007) Mater Sci Forum 534–536:897